Phys. Chem. Chem. Phys.

Does Li-Ion Transport Occur Rapidly in Localized High-Concentration Electrolytes?

Yoshifumi Watanabe,[a] Yosuke Ugata,[a,b] Kazuhide Ueno, [a,b] Masayoshi Watanabe, [b] Kaoru Dokko [a,b,*]

[a] *Department of Chemistry and Life Science, Yokohama National University, 79-5 Tokiwadai, Hodogaya-ku, Yokohama 240-8501, Japan*

[b] *Advanced Chemical Energy Research Center (ACERC), Institute of Advanced Sciences, Yokohama National University, 79-5 Tokiwadai, Hodogaya-ku, Yokohama 240-8501, Japan*

*CORRESPONDING AUTHOR

E-mail: dokko-kaoru-js@ynu.ac.jp (K.D.)

Electronic supplementary information (ESI) available.

See DOI: https://doi.org/XXXXXX

Abstract

The ionic conductivity and lithium-ion transference number of electrolytes significantly influence the rate capability of Li-ion batteries. Highly concentrated Li-salt/sulfolane (SL) electrolytes exhibit elevated Li^+ transference numbers due to lithium-ion hopping via a ligand exchange mechanism within their $–Li^+–SL–Li^+–$ network. However, highly concentrated electrolytes (HCEs) are extremely viscous and have an ionic conductivity that is one order of magnitude less than that of conventional electrolytes. Dilution of HCEs with a non-coordinating hydrofluoroether (HFE) lowers the viscosity and produces localized high-concentration electrolytes (LHCE). However, the mechanism of Li^+ transport mechanism in LHCEs is unclear. This study investigated the transport properties of LHCEs prepared by diluting a SL-based HCE with 1,1,2,2-tetrafluoroethyl-2,2,3,3-tetrafluoropropyl ether. Electrolyte viscosity decreases dramatically upon dilution, whereas ionic conductivity increases only slightly. Ion diffusivity increases with increasing HFE content due to the decrease in electrolyte viscosity. However, the Li^+ transference number declines, because the HFE interferes with conduction via the Li^+ hopping mechanism. The resulting decrease in the product of ionic conductivity and Li^+ transference number indicates superior lithium-ion transport in the parent HCE compared with LHCEs.

1. Introduction

Lithium-ion batteries (LIBs) are widely used as power sources for portable electronic devices and electric vehicles because of their high energy and power densities. Lithium-ion transport in LIBs occurs between the cathode and anode during charging and discharging, and Li^+ transport properties significantly affect the power density. The aprotic electrolyte solutions used in commercialized LIBs contain ca. 1 mol dm^{-3} (1 M) Li-salt, because ionic conductivity maximizes at about this value[1,2] However, highly concentrated electrolytes (HCEs) containing >3 M Li-salts have attracted attention in the field of battery chemistry recently, despite their lower conductivity relative to 1 M electrolytes.[3–8] The reason is that HCEs possess high thermal stability and wide electrochemical windows, which improves LIB durability. Furthermore, Li metal deposition and dissolution is highly reversible in HCEs.[9–12] Thus, HCEs are promising electrolytes for lithium metal batteries (LMBs) and possess greater energy density than current LIBs. Additionally, we recently found that certain HCEs exhibit a unique ion transport property, which involves conduction via a lithium-ion hopping mechanism.[13–18] The solvent-to-Li molar ratio decreases with increasing Li salt concentration in HCEs, because a greater fraction of the solvent participates in Li^+ solvation. Anions also are involved in Li^+ coordination, and contact ion pairs (CIPs) and ion aggregates (AGGs) form in HCEs.[3–8] In such a liquid structure, Li^+ dynamically exchanges ligands (solvent and anions) and diffuses or migrates faster than ligands, i.e., Li^+ hopping mechanism emerges. Lithium-ion hopping causes the Li^+ transference number in certain HCEs to become greater than 0.5, whereas this parameter is less than 0.3 in conventional 1 M electrolytes.[7,18] A large Li^+ transference number is advantageous in suppressing concentration polarization during high-rate charging and discharging in a battery.[19,20]

One disadvantage of HCEs is their high viscosity. The viscosity of HCEs can be greater than

100 mPa s, whereas that of typical 1 M electrolytes is less than 10 mPa s.[3–8] High viscosity produces low ionic conductivity, which can be an order of magnitude less than in 1 M electrolytes. Dilution of HCEs with non-coordinating solvents is a possible solution to this problem. We previously reported the dilution of solvate ionic liquids (SILs), which are glyme-based HCEs, with the hydrofluoroether (HFE), 1,1,2,2-tetrafluoroethyl-2,2,3,3-tetrafluoropropyl ether.[21–24] HFEs do not participate in Li^+ solvation, and the $[Li(glyme)]^+$ structure in SILs is maintained after HFE addition. The viscosity and ionic conductivity of SILs deceases and increases, respectively, upon HFE addition. We have demonstrated that Li-sulfur cells can be stably operated using HFE-diluted SIL electrolytes. Ren et al. reported the dilution of highly concentrated $LiN(SO_2F)_2$/sulfolane electrolytes with HFE[25] and designated these admixtures as "localized high-concentration electrolytes" (LHCEs).[26,27] These authors reported that a LMB ($Li/LiNi_{1/3}Mn_{1/3}Co_{1/3}O_2$) battery can function for more than 300 charge-discharge cycles with a LHCE.

Although HFE is an effective diluent that does not disrupt the Li^+ solvation structure while lowering solution viscosity, the lithium-ion transport mechanism in HFE-diluted HCEs is not fully understood. In fact, the addition of HFE only slightly increases the ionic conductivity of a HCE, whereas the LHCE viscosity is much lesser than that of the parent HCE.[16,25,28–30] In this study, we investigated the effects of HFE addition to a HCE comprising lithium bis(fluorosulfonyl)amide (LiFSA) and sulfolane (SL) (**Figure 1**). We previously reported the transport properties of highly concentrated LiFSA/SL electrolytes, which exhibit Li^+ hopping and relatively large Li^+ transference numbers (ca. 0.5).[18] In this study, an electrolyte comprising [LiFSA]/[SL] = 1/2.5 (molar ratio) was used as a model HCE, because the liquidus temperature of LiFSA/SL mixture becomes lowest at this composition (melting point: −10.4 °C) and was expected to retain its liquid state over a wide temperature range.[18,31] The viscosity, ionic conductivity, ionic diffusivity, and Li^+ transference number of HFE-diluted electrolytes were

evaluated. Finally, the effect of HFE addition on the discharge rate capability of Li/$LiCoO_2$ cells was examined.

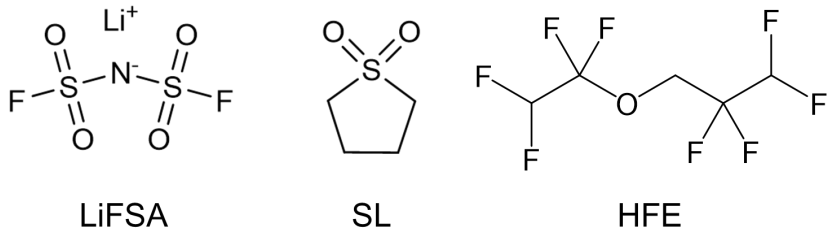

Figure 1. Chemical structures of LiFSA, SL, and HFE.

2. Experimental Section

LiFSA (Kishida Chemical), SL (Kishida Chemical), and HFE (Daikin Industries) were used as received. The electrolytes were prepared by mixing the LiFSA, SL, and HFE in [LiFSA]/[SL]/[HFE] = 1/2.5/*n* molar ratios in an Ar-filled glovebox at room temperature. Ionic conductivity (σ) was determined using an impedance analyzer (VMP-3, Bio-Logic) in the500 kHz to 1 Hz frequency range with a 10 mV root mean square (rms) voltage amplitude. A cell equipped with two platinized platinum electrodes (CG-511B, TOA Electronics) was used for conductivity measurements. The cell constant was determined in prior to measurements using a 0.01 M KCl aqueous solution at 25 °C. Density (d) and viscosity (η) were determined with a Stabinger viscometer (SVM 3000, Anton Paar). Pulsed-field gradient nuclear magnetic resonance (PFG-NMR) measurements were conducted to evaluate the diffusivities of SL, Li^+, FSA^-, and HFE in the electrolytes using a JEOL ECX-400 NMR spectrometer with a 9.4 T narrow-bore superconducting magnet equipped with a pulsed-field gradient probe and current amplifier. Detailed experimental procedures have been reported elsewhere.[15] Raman spectra of the electrolytes were collected using a 532-nm laser Raman spectrometer (NRS-4100, JASCO) calibrated with a polypropylene standard. The spectroscopic resolution was 4.6 cm^{-1}.

Lithium-ion transference numbers (t_{Li}^{abc}) of the electrolytes were evaluated under anion-blocking conditions using 2032-type coin cells. The cell was assembled in an Ar-filled glovebox. Two disk-shaped Li-metal foil electrodes (16-mm diameter, Honjyo Metal), an electrolyte (100 μL), and a glass-fiber separator (GA-55, Advantec) were encapsulated into a coin cell. Chronoamperometry of the coin cells was conducted at a constant voltage (ΔV = 10 mV). AC impedance measurements of the cells were performed immediately before and after chronoamperometry. AC impedance measurements were performed at 100 kHz to 100 mHz at 10-mV rms voltage amplitude. The t_{Li}^{abc} of the electrolytes was calculated using the equation proposed by Balasara et al.: [32]

$$t_{\mathrm{Li}}^{\mathrm{abc}} = \frac{I_{\mathrm{ss}}(\Delta V - I_{\Omega} R_{\mathrm{i},0})}{I_{\Omega}(\Delta V - I_{\mathrm{ss}} R_{\mathrm{i,ss}})}$$

where I_{ss} is the steady-state current observed by chronoamperometry, and $R_{i,0}$ and $R_{i,ss}$ are the interfacial resistances at the Li-metal electrodes measured by AC impedance before and after chronoamperometry, respectively. I_{Ω} is the current calculated using Ohm's law, $I_{\Omega} = \Delta V/(R_b + R_{i,0})$, where R_b is the bulk resistance of the electrolyte in the coin cell.

Li/$LiCoO_2$ cells were assembled to battery test the electrolytes. A cathode sheet was prepared using $LiCoO_2$ powder (Nippon Chemical Industrial Co.), acetylene black (AB, Denka), and poly(vinylidene fluoride) (PVDF, Kishida Chemical) as the active material, conductive agent, and binder, respectively. $LiCoO_2$, AB, and PVDF were mixed in an 80/10/10 mass ratio in *N*-methylpyrrolidone (NMP, Kanto Chemical) to prepare a slurry. The slurry was spread on an Al foil and dried at 80 °C overnight. The resulting cathode sheet was cut into a circular shape (13.82-mm diameter) and dried at 80 °C under vacuum overnight. The mass loading of $LiCoO_2$ on Al was 3.8–3.9 mg cm^{-2}. The Li/$LiCoO_2$ cell assembly was conducted in an Ar-filled glovebox. Lithium metal foil (16-mm diameter), a GA-55 separator (17-mm in diameter) wetted with electrolyte (100 μL), and $LiCoO_2$ were encapsulated in an

Al-coated 2032-type coin cell. Galvanostatic charge-discharge measurements on Li/$LiCoO_2$ cells were performed using an automatic charge-discharge instrument (HJ1001SD8, Hokuto Denko) at 30 °C. The specific capacities of the cells were calculated based on the mass of $LiCoO_2$.

3. Results and Discussion

Figure 2a shows the ionic conductivity (σ) and viscosity (η) of the [LiFSA]/[SL]/[HFE] = 1/2.5/n electrolytes as a function of the LiFSA concentration. Ionic conductivity increases slightly with increasing HFE content in the electrolyte and is maximal at n = 1 (2.1 M). Further addition of HFE ($n \geq$ 3) causes precipitation of the electrolyte (**Figure S1**), which might be because of the crystallization of a solid solvate. LiFSA and SL form a 1:1 solid solvate with a relatively high meting point (T_m: 75 °C).[13] The increase in ionic conductivity with increasing HFE content is attributed to the decrease in viscosity. Electrolyte viscosity decreases dramatically with increasing HFE and becomes about four times smaller at n = 1 compared with electrolyte without HFE (**Table S1**). The decrease in viscosity produces an increase in ion mobility and results in greater ionic conductivity.

Figure 2b shows the logarithmic Walden plot of molar conductivity (Λ) against reciprocal viscosity (η^{-1}). The ideal KCl line in **Figure 2b** is based on the Λ and η values of an aqueous 1 M KCl solution, wherein KCl is assumed to be completely dissociated. Molar conductivity is inversely proportional to viscosity according to the Walden rule. However, the increase in molar ionic conductivity of the HFE-diluted electrolyte is less than expected from the decrease in viscosity upon HFE addition (**Table S1**). The molar conductivity of the [LiFSA]/[SL]/[HFE] = 1/2.5/1 electrolyte is only 1.6 times greater than that of the [LiFSA]/[SL] = 1/2.5 electrolyte (n = 0), whereas the viscosity of the former is 3.8 times less than that of the latter. Ren et al. reported a similar phenomenon for the [LiFSA]/[SL]/[HFE]

= 1/3/n electrolyte.[25] The deviation of Λ from the ideal KCl line for the LiFSA/SL/HFE electrolyte becomes larger with increasing HFE molar ratio (**Figure 2b**). This result suggests that cation-anion association initiated by HFE addition is responsible. HFE has a low dielectric constant (ε_r: 6.21),[21] whereas the ε_r of SL is 43.3.[33] Thus, the attractive interaction between Li^+ and FSA^- is enhanced by addition of a low polar solvent.

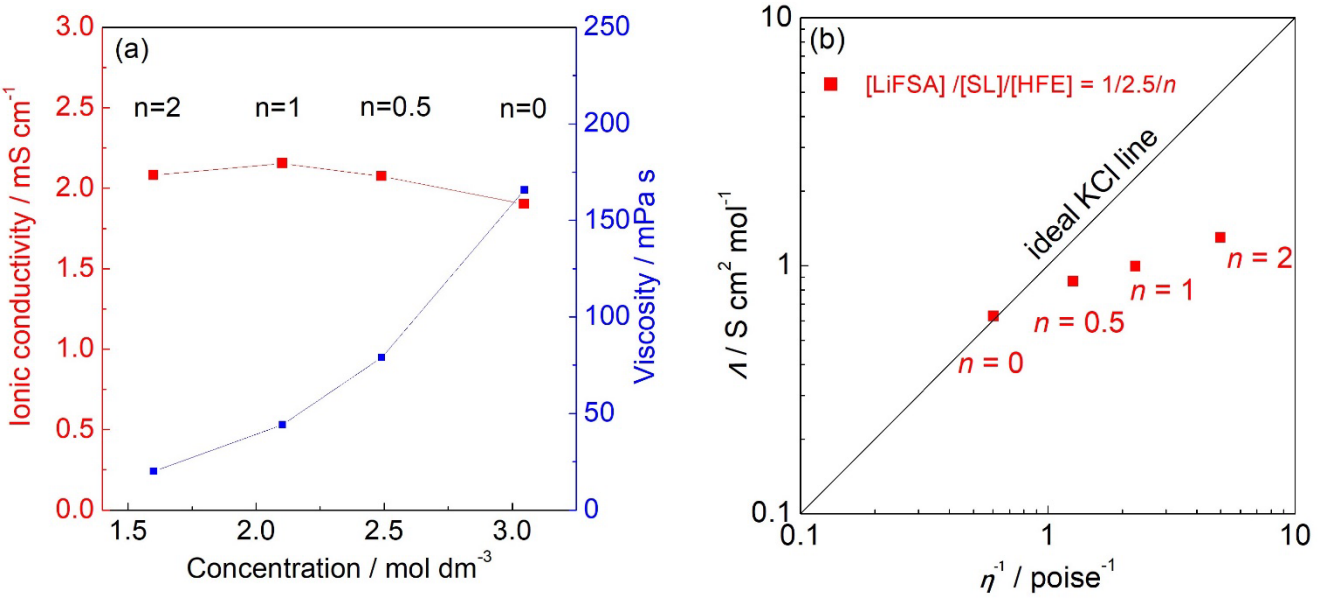

Figure 2. (a) Ionic conductivity and viscosity as a function of LiFSA concentration and (b) Walden plot of the [LiFSA]/[SL]/[HFE] = 1/2.5/n electrolytes at 30 ºC.

Raman spectroscopy was used to investigate changes in the liquid structure upon HFE addition. **Figure 3a** shows Raman spectra of the electrolytes at 540–600 cm^{-1}. The peak at 568 cm^{-1} for neat SL is assigned to the O–S–O scissoring vibration of SL. This peak shifts to higher wavenumbers upon complexation with Li^+. We previously reported Raman spectra of highly concentrated Li-salt/SL electrolytes.[13,16] Lithium ions coordinate to the oxygen atoms of the SL sulfonyl group. When a single SL oxygen atom coordinates to a single Li^+ (monodentate coordination), the peak shifts to 571 cm^{-1}. In highly concentrated electrolytes, the two SL oxygen atoms bind to different Li^+ ions (bridging-type

coordination), and the O–S–O vibration occurs at ~580 cm^{-1}. **Figure 3a** shows that the sulfolane O–S–O vibration in [LiFSA]/[SL] = 1/2.5 electrolyte is blue shifted with a broad peak extending to ~590 cm^{-1}, which suggests the coexistence of monodentate and bridging SL coordination in the electrolyte. The coordination number of Li^+ is typically 4–5 in liquid electrolytes.[34–36] This value cannot be attained if each SL molecule is coordinated to merely a single Li^+ in the [LiFSA]/[SL] = 1/2.5 electrolyte. Therefore, some SL molecules, in addition to being bound to lithium ions in a monodentate manner, must act as bridging ligands to form a $\cdots Li^+ \cdots SL \cdots Li^+ \cdots$ network. In addition, FSA^- might coordinate to Li^+ in the [LiFSA]/[SL] = 1/2.5 electrolyte. **Figure 3b** shows Raman spectra corresponding to the S–N–S stretching vibration of FSA^- at 700–770 cm^{-1}. Free FSA^-exhibits a peak at 724–730 cm^{-1}.[15,37,38] This signal shifts to higher wavenumbers upon complexing with Li^+ to form contact ion pairs (CIPs) and larger ionic aggregates (AGGs). The S–N–S vibration is observed at ~731 cm^{-1} in the [LiFSA]/[SL] = 1/2.5 electrolyte, which indicates that the majority of FSA^- anions form CIPs and AGGs with Li ions in the electrolyte. Because the bridging SL molecules described above link different CIPs, $[Li_x(SL)_yFSA_z]^{x-z}$ ionic clusters become established in the electrolyte.

Addition of HFE to [LiFSA]/[SL] = 1/2.5 blue shifts both the O–S–O scissoring vibration of SL and the S–N–S stretching vibration of FSA^-, indicating that the attractive Li^+–SL and Li^+– FSA^- interactions are enhanced. HFE does not solvate Li^+.[16,22,25] Thus, no spectral change was observed for neat HFE nor for the electrolytes. Ren et al. conducted ab initio molecular dynamics simulations of [LiFSA]/[SL]/[HFE] = 1/3/3 and reported that HFE is not involved in Li^+ solvation.[25] Therefore, we assume that addition of HFE results in fragmentation of the $\cdots Li^+ \cdots SL \cdots Li^+ \cdots$ network creating isolated ionic clusters. This structural change strengthens the electrostatic Li^+–SL and Li^+– FSA^- interactions within the clusters that are surrounded by a low polar HFE molecules.

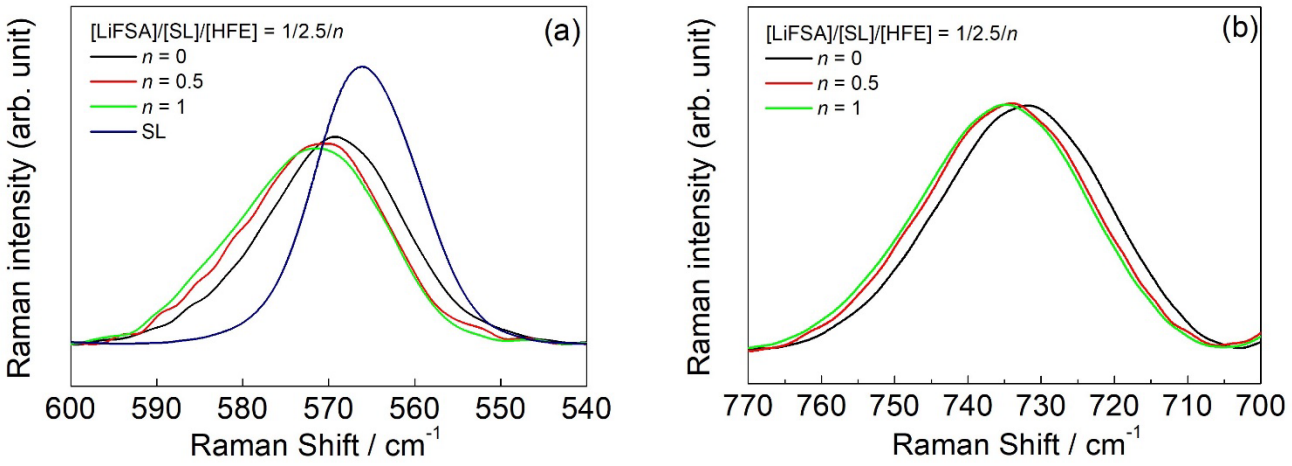

Figure 3. Raman spectra of (a) O–S–O scissoring vibration of SL (540–600 cm^{-1}) and (b) S–N–S symmetric stretching vibration of FSA^- (700–770 cm^{-1}) in [LiFSA]/[SL]/[HFE] electrolytes at room temperature.

Figure 4 shows the diffusivities of Li^+ (D_{Li}), SL (D_{SL}), FSA^- (D_{FSA}), and HFE (D_{HFE}) in [LiFSA]/[SL]/[HFE] = 1/2.5/*n* electrolytes. The diffusivity of each component increases with increasing HFE, because the viscosity of the electrolyte decreases. In [LiFSA]/[SL] = 1/2.5, Li^+ diffuses faster than SL and FSA^-. Here, almost all SL molecules and some FSA anions are coordinated to Li^+. In this highly concentrated electrolyte, Li^+ diffusion is accompanied by dynamic exchange of its SL and FSA^- ligands within the $\cdots Li^+ \cdots SL \cdots Li^+ \cdots$ network. In other words, conduction occurs via Li^+ hopping.[13,16–18] This process endows Li^+ with the fastest rate of diffusion ($D_{SL} < D_{FSA} < D_{Li}$) among the components of the [LiFSA]/[SL] = 1/2.5 electrolyte. However, D_{Li} becomes small relative to D_{SL} and D_{FSA} as the HFE content increases. In electrolytes with $n \geq 1$, the order of diffusivities is $D_{Li} < D_{FSA} < D_{SL} < D_{HFE}$. Thus, the mechanism of Li^+ transport is affected by the addition of HFE. Lithium-ion ligand exchange may be interrupted by HFE, because Li^+ does not coordinate HFE. According to the Stokes–Einstein equation, which is valid for the diffusion of species in a continuous medium, diffusion coefficients are proportional to $1/\eta$ and $1/r_h$, where r_h is the hydrodynamic radius of the diffusing species. However, D_{Li} in

[LiFSA]/[SL]/[HFE] = 1/2.5/1 is only 1.5 times greater than that in [LiFSA]/[SL] = 1/2.5 (**Table S2**), although the viscosity of the former is 3.8 times less than that of the latter (**Table S1**). This is one of the reasons why the molar ionic conductivity of [LiFSA]/[SL]/[HFE] = 1/2.5/1 is less than the value expected from the lower viscosity of the HFE-diluted electrolyte (**Figure 2b**). A possible explanation is that the hydrodynamic radii of the ions become larger upon HFE addition. Dilution of HCE with HFE causes fragmentation of the $\cdots Li^+ \cdots SL \cdots Li^+ \cdots$ network and impedes the exchange of SL and FSA^- ligands between different ionic clusters (**Figure 5**), which prolongs the lifetimes for the ionic clusters in the electrolyte. The cations, anions, and SL molecules comprising the clusters remain intact for longer times and diffuse together over longer distances in the HFE-diluted electrolyte. Thus, the hydrodynamic radii of diffusing species are larger and the contribution of Li^+ hopping to the conduction mechanism is decreased by the addition of HFE.

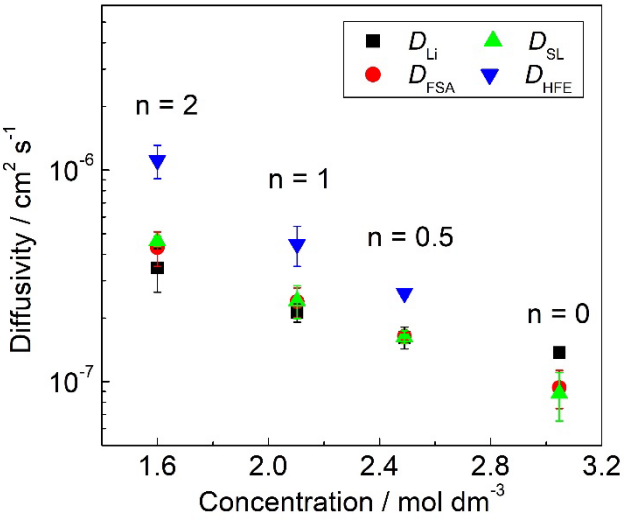

Figure 4. Diffusivities of Li^+ (D_{Li}), FSA^- (D_{FSA}), SL (D_{SL}), and HFE (D_{HFE}) in [LiFSA]/[SL]/[HFE] = 1/2.5/*n* electrolytes at 30 ºC.

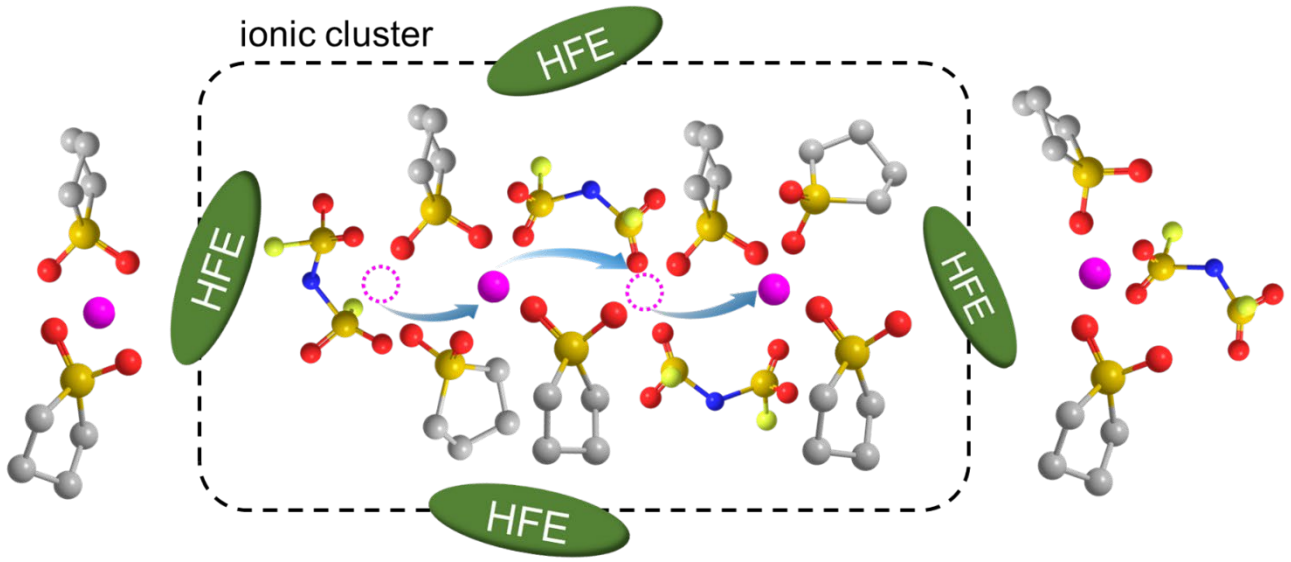

Figure 5. Schematic illustration of Li^+ ligand exchange in [LiFSA]/[SL]/[HFE] = 1/2.5/*n* electrolytes.

The molar conductivity (Λ_{NE}) of an electrolyte solution can be calculated from the diffusivities of ions by use of the Nernst–Einstein relation,

$$\Lambda_{NE} = \frac{F^2}{RT}(D_{Li} + D_{FSA})$$

where *F* is the Faraday constant, *R* is the gas constant, and *T* is the absolute temperature. Note that Λ_{NE} is calculated based on the assumption that the Li-salt is completely dissociated and the motions of the ions in the solution are not correlated (i.e., there are no ion-ion interactions). The inverse Haven ratio (Λ/Λ_{NE}), or "ionicity,"[39] reflects the correlated motion of ions in an electrolyte.[40] **Figure 6** shows a plot of Λ/Λ_{NE} for [LiFSA]/[SL]/[HFE] = 1/2.5/*n* electrolytes as a function of LiFSA concentration. Λ/Λ_{NE} values for binary [LiFSA]/[SL] = 1/*m* electrolytes at various molar ratios are shown for comparison. The Λ/Λ_{NE} values decrease with increasing HFE content (decreasing LiFSA concentration). This is attributed to the correlated movement of Li^+ and FSA^- in the same direction. As indicated above, the lifetime of $[Li_x(SL)_yFSA_z]^{x-z}$ clusters is prolonged by the addition of HFE, which enhances the correlated motion of Li^+ and FSA^-. Correlated Li^+–FSA^- motion has a negative impact on the molar conductivity,[40] and results

in a decrease in Λ/Λ_{NE}. In contrast, the Λ/Λ_{NE} values of binary [LiFSA]/[SL] = 1/m electrolytes increase slightly with decreasing LiFSA concentration. Dilution with polar SL solvent divides the $[Li_x(SL)_yFSA_z]^{x-z}$ clusters into FSA^- anions and solvated Li^+ ions, $[Li(SL)_s]^+$, where s is the Li^+ solvation number. At low electrolyte concentrations, electrostatic interaction between FSA^- and solvated Li^+ is weakened by the increase in high-dielectric SL content and the degree of correlated ionic motion is reduced.

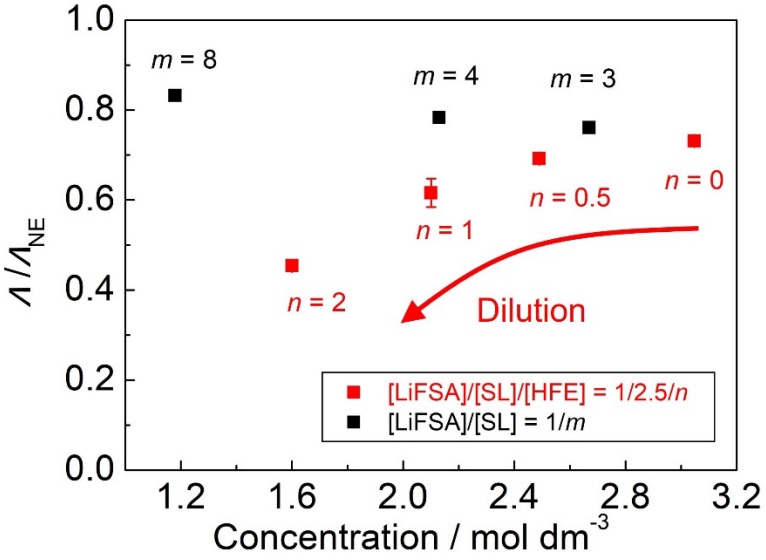

Figure 6. Λ/Λ_{NE} in [LiFSA]/[SL]/[HFE] = 1/2.5/n electrolytes and [LiFSA]/[SL] = 1/m electrolytes as a function of LiFSA concentration at 30 ºC. Λ/Λ_{NE} values for the [LiFSA]/[SL] electrolytes were calculated from the data in Ref. [13].

Li^+ transference numbers, t_{Li}^{abc}, were evaluated using symmetric Li/Li cells (**Figure S2**) to investigate the Li^+ transport properties of [LiFSA]/[SL]/[HFE] = 1/2.5/n electrolytes under anion-blocking conditions. **Figure 7** plots the t_{Li}^{abc} values of [LiFSA]/[SL]/[HFE] = 1/2.5/n electrolytes as a function of LiFSA concentration. In the HFE-free [LiFSA]/[SL] = 1/2.5, t_{Li}^{abc} is relatively high (0.53), due to lithium-ion hopping conduction via Li^+ ligand exchange.[13] However, t_{Li}^{abc} decreases gradually with increasing HFE content, because of the interruption of the ligand exchange process. The product of ionic conductivity σ and t_{Li}^{abc} is also shown in **Figure 7**. Although ionic conductivity increases slightly

upon HFE addition (**Figure 2**), $\sigma \times t_{Li}^{abc}$ decreases gradually. This indicates that Li^+ transport in HFE-diluted electrolytes under anion-blocking conditions is diminished relative to HFE-free electrolytes despite the greater ionic conductivity of the former.

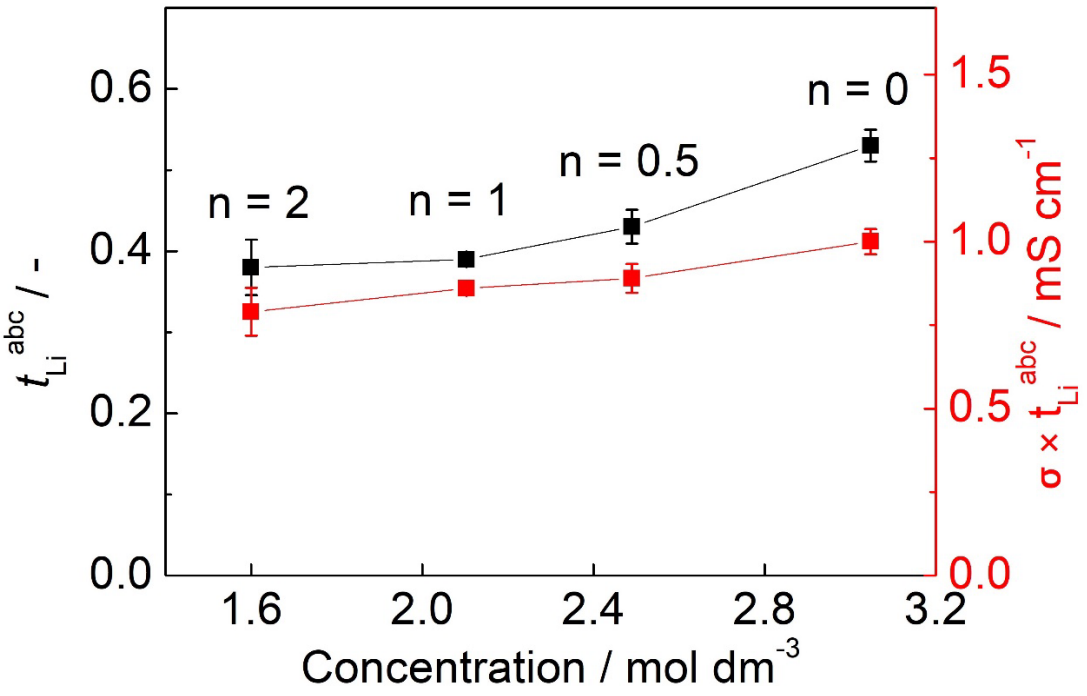

Figure 7. Li^+ transference number, t_{Li}^{abc}, under anion-blocking conditions and the product of ionic conductivity, σ, and t_{Li}^{abc} as a function of LiFSA concentration in [LiFSA]/[SL]/[HFE] = 1/2.5/*n* electrolytes at 30 ºC.

Galvanostatic charge-discharge measurements on Li/$LiCoO_2$ cells with [LiFSA]/[SL]/[HFE] = 1/2.5/*n* electrolytes were conducted to investigate the effect of HFE dilution on the performance of LMBs. [LiFSA]/[SL]/[HFE] = 1/2.5/*n* electrolytes are oxidatively stable up to 4.2 V versus Li/Li^+ (**Figure S3**). Reversible Li deposition and dissolution are possible in these electrolytes owing to the formation of a solid-electrolyte interphase (SEI) on the Li electrode (**Figures S4–S6**).[25] Typical porous polyolefin-film separators in LIBs are poorly wetted by [LiFSA]/[SL] = 1/2.5, which adversely affects battery performance. Although wettability can be improved by the addition of HFE, which is an advantage of

HFE-diluted electrolytes in battery applications,[25–27] we used a 90%-porous glass fiber filter (GA-55) as a separator between the Li metal anode and $LiCoO_2$ cathode. The GA-55 filter is wettable by both HFE-free and HFE-diluted electrolytes. **Figure 8** shows the discharge capacities of Li/$LiCoO_2$ cells with [LiFSA]/[SL]/[HFE] = 1/2.5/*n* electrolytes as a function of current density. All cells exhibited similar discharge capacities (ca. 140 mAh g^{-1}), which are close to the theoretical capacity of $LiCoO_2$ at low current density (0.05 mA cm^{-2}). The discharge capacity of each cell decreased gradually with increasing current density. At current densities above 10 mA cm^{-2}, the capacities of cells with HFE-diluted electrolytes are slightly smaller than that of the cell with HFE-free electrolyte. This might be due to the diminished Li^+ transport in HFE-diluted electrolytes compared to that in the HFE-free medium under anion-blocking conditions. The $\sigma \times t_{Li}^{abc}$ values of HFE-diluted electrolytes are lesser than that of the HFE-free electrolyte (**Figure 7**). Additionally, t_{Li}^{abc} significantly impacts the development of a concentration gradient in the electrolyte during discharge.[19,20] The lower t_{Li}^{abc} values in HFE-diluted electrolytes are less effective in suppressing concentration polarization in the cells during discharging at high current densities. At current densities above 10 mA cm^{-2}, the slope of the discharge curve for the cell with [LiFSA]/[SL]/[HFE] = 1/2.5/1 becomes slightly steeper than that of the cell with [LiFSA]/[SL] = 1/2.5 (**Figure S7**). This difference indicates that the concentration overpotential is larger due to the steeper concentration gradient in the former cell. When the concentration gradient becomes very steep, depletion of the Li-salt in the porous cathode leads to the lower utilization of the $LiCoO_2$ active material. Consequently, the rate capability of the Li/$LiCoO_2$ cell containing the HFE-free electrolyte having a higher t_{Li}^{abc} is superior to that of the cell containing a HFE-diluted electrolyte.

The dilution of HCEs with a non-coordinating solvent does not always enhance Li^+ transport under anion-blocking conditions. An optimum battery electrolyte should possess a high ionic

conductivity and a large Li^+ transference number. The transport properties of LHCEs depend on the physicochemical properties of the diluent and the parent HCE. The salt concentration, Li salt anion, and solvent structure in the parent HCE significantly influence the transport properties of LHCEs. Interactions between the diluent and Li salt also affect Li^+ ion transport. To achieve both a high ionic conductivity and high Li^+ transference number with a LHCE, a weakly coordinating diluent instead of non-coordinating HFE may be advisable. A non-coordinating HFE interrupts Li^+ ligand exchange and decreases the t_{Li}^{abc} in the electrolyte. Diluents with weaker coordination abilities than SL and the electrolyte anion will decrease viscosity and increase ionic conductivity without interrupting Li^+ ligand exchange. Further study is needed to identify such diluents and to develop a liquid electrolyte possessing both high σ and high t_{Li}^{abc}.

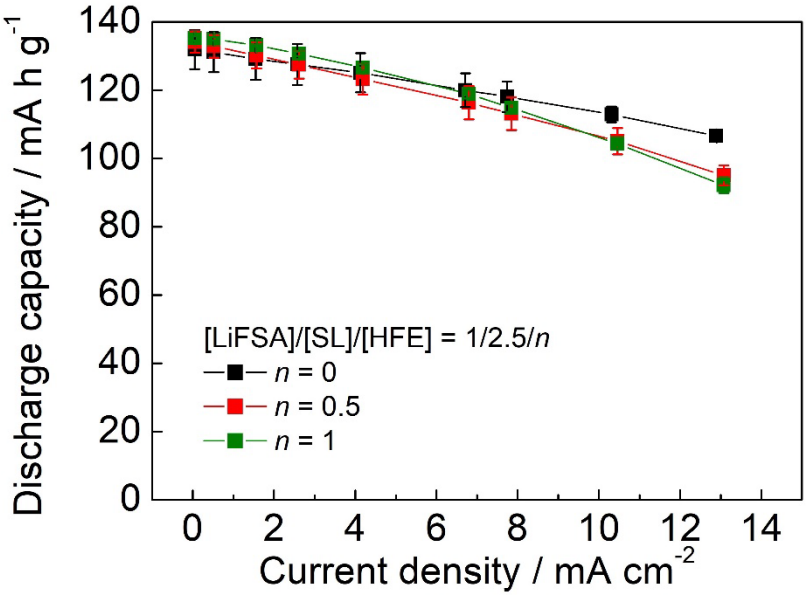

Figure 8. Discharge capacities of Li/$LiCoO_2$ cells with [LiFSA]/[SL]/[HFE] = 1/2.5/*n* electrolytes as a function of current density at 30 ºC. The cells were charged to 4.2 V at 0.05 mA cm^{-2} prior to each discharge.

4. Conclusion

The lithium-ion transport properties of [LiFSA]/[SL]/[HFE] = 1/2.5/n electrolytes have been investigated. A $\cdots Li^+ \cdots SL \cdots Li^+ \cdots$ network structure in [LiFSA]/[SL] =1/2.5 electrolyte promotes the dynamic exchange of ligands of Li^+ and ionic conduction via a Li^+ hopping mechanism. The resulting Li^+ transference number, t_{Li}^{abc}, is relatively high. Dilution of a high-concentration electrolyte with HFE dramatically decreases the viscosity and slightly increases the ionic conductivity and diffusivity. Addition of HFE to [LiFSA]/[SL] = 1/2.5 fragments the network structure and interrupts Li^+ ligand exchange, which lowers t_{Li}^{abc}. Thus, Li^+ transport characterized by $\sigma \times t_{Li}^{abc}$ in HFE-diluted electrolytes is less than that in HFE-free electrolyte under anion-blocking conditions. The lower t_{Li}^{abc} of HFE-diluted electrolytes is less effective in suppressing concentration polarization in the cell during charging and discharging of a Li metal battery at high current densities. Consequently, the rate capability of a Li metal battery with HFE-free electrolyte is superior to that of batteries with a HFE-diluted electrolyte.

Conflicts of interest

There are no conflicts to declare.

Acknowledgments.

This study was partially supported by JSPS KAKENHI (grant no. JP19H05813, JP21H04697, JP22H00340) from the Japan Society for the Promotion of Science (JSPS) and by JST ALCA-SPRING Grant Number JPMJAL1301.

References

(1) Xu, K. Nonaqueous Liquid Electrolytes for Lithium-Based Rechargeable Batteries. *Chem. Rev.* **2004**, *104*, 4303–4417.

(2) Xu, K. Electrolytes and Interphases in Li-Ion Batteries and Beyond. *Chem. Rev.* **2014**, *114*, 11503–11618.

(3) Yamada, Y.; Yamada, A. Review—Superconcentrated Electrolytes for Lithium Batteries. *J. Electrochem. Soc.* **2015**, *162*, A2406–A2423.

(4) Yamada, Y.; Wang, J.; Ko, S.; Watanabe, E.; Yamada, A. Advances and Issues in Developing Salt-Concentrated Battery Electrolytes. *Nat. Energy* **2019**, *4*, 269–280.

(5) Borodin, O.; Self, J.; Persson, K. A.; Wang, C.; Xu, K. Uncharted Waters: Super-Concentrated Electrolytes. *Joule* **2020**, *4*, 69–100.

(6) Li, M.; Wang, C.; Chen, Z.; Xu, K.; Lu, J. New Concepts in Electrolytes. *Chem. Rev.* **2020**, *120*, 6783–6819.

(7) Ugata, Y.; Shigenobu, K.; Tatara, R.; Ueno, K.; Watanabe, M.; Dokko, K. Solvate Electrolytes for Li and Na Batteries: Structures, Transport Properties, and Electrochemistry. *Phys. Chem. Chem. Phys.* **2021**, *23*, 21419–21436.

(8) Sayah, S.; Ghosh, A.; Baazizi, M.; Amine, R.; Dahbi, M.; Amine, Y.; Ghamouss, F.; Amine, K. How Do Super Concentrated Electrolytes Push the Li-Ion Batteries and Supercapacitors beyond Their Thermodynamic and Electrochemical Limits? *Nano Energy* **2022**, *98*, 107336.

(9) Suo, L.; Hu, Y. S.; Li, H.; Armand, M.; Chen, L. A New Class of Solvent-in-Salt Electrolyte for High-Energy Rechargeable Metallic Lithium Batteries. *Nat. Commun.* **2013**, *4*, 1481.

(10) Qian, J.; Henderson, W. A.; Xu, W.; Bhattacharya, P.; Engelhard, M.; Borodin, O.; Zhang, J. G.

High Rate and Stable Cycling of Lithium Metal Anode. *Nat. Commun.* **2015**, *6*, 6362.

(11) Fan, X.; Chen, L.; Ji, X.; Deng, T.; Hou, S.; Chen, J.; Zheng, J.; Wang, F.; Jiang, J.; Xu, K.; Wang, C. Highly Fluorinated Interphases Enable High-Voltage Li-Metal Batteries. *Chem* **2018**, *4*, 174–185.

(12) Zeng, Z.; Murugesan, V.; Han, K. S.; Jiang, X.; Cao, Y.; Xiao, L.; Ai, X.; Yang, H.; Zhang, J. G.; Sushko, M. L.; Liu, J. Non-Flammable Electrolytes with High Salt-to-Solvent Ratios for Li-Ion and Li-Metal Batteries. *Nat. Energy* **2018**, *3*, 674–681.

(13) Dokko, K.; Watanabe, D.; Ugata, Y.; Thomas, M. L.; Tsuzuki, S.; Shinoda, W.; Hashimoto, K.; Ueno, K.; Umebayashi, Y.; Watanabe, M. Direct Evidence for Li Ion Hopping Conduction in Highly Concentrated Sulfolane-Based Liquid Electrolytes. *J. Phys. Chem. B* **2018**, *122*, 10736–10745.

(14) Kondou, S.; Thomas, M. L.; Mandai, T.; Ueno, K.; Dokko, K.; Watanabe, M. Ionic Transport in Highly Concentrated Lithium Bis(Fluorosulfonyl)Amide Electrolytes with Keto Ester Solvents: Structural Implications for Ion Hopping Conduction in Liquid Electrolytes. *Phys. Chem. Chem. Phys.* **2019**, *21*, 5097–5105.

(15) Ugata, Y.; Thomas, M. L.; Mandai, T.; Ueno, K.; Dokko, K.; Watanabe, M. Li-Ion Hopping Conduction in Highly Concentrated Lithium Bis(Fluorosulfonyl)Amide/Dinitrile Liquid Electrolytes. *Phys. Chem. Chem. Phys.* **2019**, *21*, 9759–9768.

(16) Nakanishi, A.; Ueno, K.; Watanabe, D.; Ugata, Y.; Matsumae, Y.; Liu, J.; Thomas, M. L.; Dokko, K.; Watanabe, M. Sulfolane-Based Highly Concentrated Electrolytes of Lithium Bis(Trifluoromethanesulfonyl)Amide: Ionic Transport, Li-Ion Coordination and Li-S Battery Performance. *J. Phys. Chem. C* **2019**, *123*, 14229–14238.

(17) Ugata, Y.; Sasagawa, S.; Tatara, R.; Ueno, K.; Watanabe, M.; Dokko, K. Structural Effects of Solvents on Li-Ion-Hopping Conduction in Highly Concentrated $LiBF_4$/Sulfone Solutions. *J. Phys. Chem. B* **2021**, *125*, 6600–6608.

(18) Ugata, Y.; Chen, Y.; Sasagawa, S.; Ueno, K.; Watanabe, M.; Mita, H.; Shimura, J.; Nagamine, M.; Dokko, K. Eutectic Electrolytes Composed of $LiN(SO_2F)_2$ and Sulfones for Li-Ion Batteries. *J. Phys. Chem. C* **2022**, *126*, 10024–10034.

(19) Doyle, M.; Fuller, T. F.; Newman, J. The Importance of the Lithium Ion Transference Number in Lithium/Polymer Cells. *Electrochim. Acta* **1994**, *39*, 2073–2081.

(20) Diederichsen, K. M.; McShane, E. J.; McCloskey, B. D. Promising Routes to a High Li^+ Transference Number Electrolyte for Lithium Ion Batteries. *ACS Energy Lett.* **2017**, *2*, 2563–2575.

(21) Dokko, K.; Tachikawa, N.; Yamauchi, K.; Tsuchiya, M.; Yamazaki, A.; Takashima, E.; Park, J.-W.; Ueno, K.; Seki, S.; Serizawa, N.; Watanabe, M. Solvate Ionic Liquid Electrolyte for Li–S Batteries. *J. Electrochem. Soc.* **2013**, *160*, A1304–A1310.

(22) Moon, H.; Mandai, T.; Tatara, R.; Ueno, K.; Yamazaki, A.; Yoshida, K.; Seki, S.; Dokko, K.; Watanabe, M. Solvent Activity in Electrolyte Solutions Controls Electrochemical Reactions in Li-Ion and Li-Sulfur Batteries. *J. Phys. Chem. C* **2015**, *119*, 3957–3970.

(23) Ueno, K.; Murai, J.; Ikeda, K.; Tsuzuki, S.; Tsuchiya, M.; Tatara, R.; Mandai, T.; Umebayashi, Y.; Dokko, K.; Watanabe, M. Li+ Solvation and Ionic Transport in Lithium Solvate Ionic Liquids Diluted by Molecular Solvents. *J. Phys. Chem. C* **2016**, *120*, 15792–15802.

(24) Sudoh, T.; Shigenobu, K.; Dokko, K.; Watanabe, M.; Ueno, K. Li+ Transference Number and Dynamic Ion Correlations in Glyme-Li Salt Solvate Ionic Liquids Diluted with Molecular

Solvents. *Phys. Chem. Chem. Phys.* **2022**, *24*, 14269–14276.

(25) Ren, X.; Chen, S.; Lee, H.; Mei, D.; Engelhard, M. H.; Burton, S. D.; Zhao, W.; Zheng, J.; Li, Q.; Ding, M. S.; Schroeder, M.; Alvarado, J.; Xu, K.; Meng, Y. S.; Liu, J.; Zhang, J. G.; Xu, W. Localized High-Concentration Sulfone Electrolytes for High-Efficiency Lithium-Metal Batteries. *Chem* **2018**, *4*, 1877–1892.

(26) Chen, S.; Zheng, J.; Mei, D.; Han, K. S.; Engelhard, M. H.; Zhao, W.; Xu, W.; Liu, J.; Zhang, J. G. High-Voltage Lithium-Metal Batteries Enabled by Localized High-Concentration Electrolytes. *Adv. Mater.* **2018**, *30*, 1–7.

(27) Cao, X.; Jia, H.; Xu, W.; Zhang, J.-G. Review—Localized High-Concentration Electrolytes for Lithium Batteries. *J. Electrochem. Soc.* **2021**, *168*, 010522.

(28) Terada, S.; Susa, H.; Tsuzuki, S.; Mandai, T.; Ueno, K.; Dokko, K.; Watanabe, M. Glyme-Sodium Bis(Fluorosulfonyl)Amide Complex Electrolytes for Sodium Ion Batteries. *J. Phys. Chem. C* **2018**, *122*, 16589–16599.

(29) Shin, M.; Wu, H. L.; Narayanan, B.; See, K. A.; Assary, R. S.; Zhu, L.; Haasch, R. T.; Zhang, S.; Zhang, Z.; Curtiss, L. A.; Gewirth, A. A. Effect of the Hydrofluoroether Cosolvent Structure in Acetonitrile-Based Solvate Electrolytes on the Li+ Solvation Structure and Li-S Battery Performance. *ACS Appl. Mater. Interfaces* **2017**, *9*, 39357–39370.

(30) Takada, K.; Yamada, Y.; Yamada, A. Optimized Nonflammable Concentrated Electrolytes by Introducing a Low-Dielectric Diluent. *ACS Appl. Mater. Interfaces* **2019**, *11*, 35770–35776.

(31) Maeyoshi, Y.; Ding, D.; Kubota, M.; Ueda, H.; Abe, K.; Kanamura, K.; Abe, H. Long-Term Stable Lithium Metal Anode in Highly Concentrated Sulfolane-Based Electrolytes with Ultrafine Porous Polyimide Separator. *ACS Appl. Mater. Interfaces* **2019**, *11*, 25833–25843.

(32) Galluzzo, M. D.; Maslyn, J. A.; Shah, D. B.; Balsara, N. P. Ohm's Law for Ion Conduction in Lithium and beyond-Lithium Battery Electrolytes. *J. Chem. Phys.* **2019**, *151*, 020901.

(33) Casteel, J. F.; Sears, P. G. Dielectric Constants, Viscosities, and Related Physical Properties of 10 Liquid Sulfoxides and Sulfones at Several Temperatures. *J. Chem. Eng. Data* **1974**, *19*, 196–200.

(34) Hyodo, S.-A.; Okabayashi, K. Raman Intensity Study of Local Structure in Non-Aqueous Electrolyte Solutions—I. Cation-Solvent Interaction in $LiClO_4$/Ethylene Carbonate. *Electrochim. Acta* **1989**, *34*, 1551–1556.

(35) Morita, M.; Asai, Y.; Yoshimoto, N.; Ishikawa, M. A Raman Spectroscopic Study of Organic Electrolyte Solutions Based on Binary Solvent Systems of Ethylene Carbonate with Low Viscosity Solvents Which Dissolve Different Lithium Salts. *J. Chem. Soc. Faraday Trans.* **1998**, *94*, 3451–3456.

(36) Kameda, Y.; Umebayashi, Y.; Takeuchi, M.; Wahab, M. A.; Fukuda, S.; Ishiguro, S.; Sasaki, M.; Amo, Y.; Usuki, T. Solvation Structure of Li^+ in Concentrated $LiPF_6$-Propylene Carbonate Solutions. *J. Phys. Chem. B* **2007**, *111*, 6104–6109.

(37) Fujii, K.; Hamano, H.; Doi, H.; Song, X.; Tsuzuki, S.; Hayamizu, K.; Seki, S.; Kameda, Y.; Dokko, K.; Watanabe, M.; Umebayashi, Y. Unusual Li^+ Ion Solvation Structure in Bis(Fluorosulfonyl)Amide Based Ionic Liquid. *J. Phys. Chem. C* **2013**, *117*, 19314–19324.

(38) Han, S.; Borodin, O.; Seo, D. M.; Zhou, Z.; Henderson, W. A. Electrolyte Solvation and Ionic Association V. Acetonitrile-Lithium Bis(Fluorosulfonyl)Imide (LiFSI) Mixtures. *J. Electrochem. Soc.* **2014**, *161*, A2042–A2053.

(39) Ueno, K.; Tokuda, H.; Watanabe, M. Ionicity in Ionic Liquids: Correlation with Ionic Structure

and Physicochemical Properties. *Phys. Chem. Chem. Phys.* **2010**, *12*, 1649–1658.

(40) Vargas-Barbosa, N. M.; Roling, B. Dynamic Ion Correlations in Solid and Liquid Electrolytes: How Do They Affect Charge and Mass Transport? *ChemElectroChem* **2020**, *7*, 367–385.